Emerging Materials and Design Principles for Wurtzite-type Ferroelectrics

Cheng-Wei Lee,[a*] Naseem Ud Din,[a] Keisuke Yazawa,[a,b] Geoff L. Brennecka,[a] Andriy Zakutayev,[b] Prashun Gorai [a,b*]

The energy demand for computing and data storage will continue to rise exponentially unless non-traditional computing architectures and innovative storage solutions are explored. Low-energy computing, including compute-in-memory architectures, has the potential to address these energy and environmental challenges and, in particular, tetrahedral (wurtzite-type) ferroelectrics are promising options for both performance and integration with existing semiconductor processes. The $Al_{1-x}Sc_xN$ alloy is among the few tetrahedral materials that exhibit ferroelectric switching, but the electric field required to switch the polarization i.e., the coercive field, E_c, is on the order of MV/cm, which is about 1-2 orders of magnitude higher than more traditional oxide perovskite ferroelectrics (E_c < 100 kV/cm). Instead of further engineering $Al_{1-x}Sc_xN$ and related alloys, we explore the alternative route of computationally identifying new materials with switching barriers lower than AlN while still possessing high enough intrinsic breakdown fields. Going beyond binary compounds, we explore the search space of multinary compounds with wurtzite-type structures. Through this large-scale search, we identify four promising ternary nitrides and oxides, including Mg_2PN_3, $MgSiN_2$, Li_2SiO_3, and Li_2GeO_3, for future experimental realization and engineering. In >90% of the considered multinary materials, we identify unique switching pathways and non-polar structures that are distinct from the commonly assumed switching mechanism in AlN-based materials. Our results disprove the existing design principle based on reduction of wurtzite c/a lattice parameter ratio while supporting two emerging design principles — ionicity and bond strength.

1 Introduction

With an increasingly digitized world, data centers and computing needs increase their energy consumption and carbon footprint.[1,2] The computational share of energy consumption in the last decade plateaued at about 1% of global energy consumption, thanks to improvements in efficiency and adoption of cloud computing.[3] However, these improvements are expected to reach their limit soon[3,4] while the growth in data centers and computing needs are expected to continue.[5] Therefore, breakthroughs in energy-efficient computing, data storage, and communication are critical for minimizing the associated environmental impacts.

Ferroelectrics maintain a spontaneous electric polarization without the need for constant external energy, and the direction of this polarization can be switched on demand via the application of an electric field. These two key features make ferroelectrics promising materials for energy-efficient data storage in comparison to dynamic random access memory[6] and for neuromorphic computing and related memory-logic hybrids, which need simultaneous and colocated data storage and information processing.[7–9] Recently discovered tetrahedral (wurtzite-type) ferroelectrics are of particular interest because of the relative ease of direct and high-quality integration with existing and emerging tetrahedral semiconductors (e.g., Si, GaAs, GaN, SiC, AlN).[6,10]

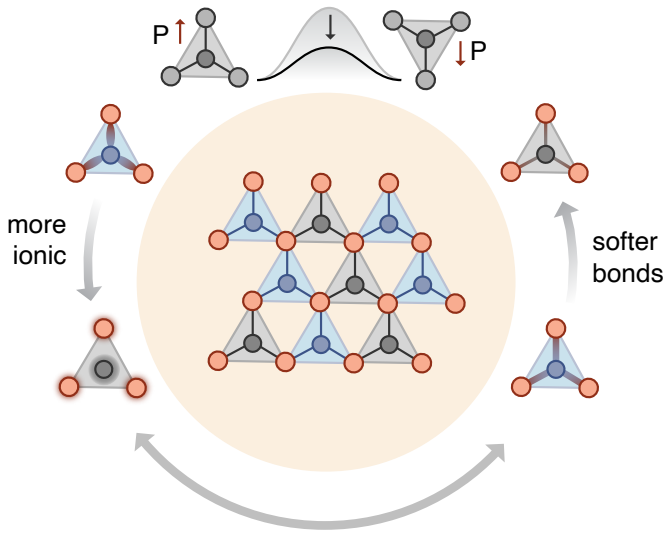

Fig. 1 Emerging design principles for discovery and engineering of multinary tetrahedral (wurtzite-type) ferroelectrics with lower coercive fields. More ionic and softer bonds lower polarization switching barriers.

It has long been recognized that wurtzite-type structures possess very large spontaneous polarization, often > 100 $\mu C/cm^2$,[11] but it was not until Fichtner et al. demonstrated in 2019 that

[a]*Colorado School of Mines, Golden, CO 80401.* [b]*National Renewable Energy Laboratory, Golden, CO 80401.* *E-mail: clee2@mines.edu, pgorai@mines.edu*

the polarization of $Al_{1-x}Sc_xN$ could be reversed under an applied electric field prior to dielectric breakdown[10] that tetrahedrally-bonded materials were acknowledged as potentially ferroelectric. In recent years, robust ferroelectricity has also been demonstrated in $Al_{1-x}B_xN$, $Ga_{1-x}Sc_xN$, and $Zn_{1-x}Mg_xO$.[12–15] The large spontaneous polarization values of these tetrahedrally-bonded ferroelectrics are of interest for neuromorphic architectures and open up the possibility of multi-state bits,[16,17] but the coercive fields – and therefore switching voltages – are still one to two orders of magnitude higher than ideal.[18]

Instead of approaching the challenge via engineering existing materials like $Al_{1-x}Sc_xN$ and $Zn_{1-x}Mg_xO$ alloys, we adopted the alternative approach to computationally identify new multinary wurtzite-type ferroelectrics. The idea is to identify new materials with suitable initial properties (low barrier for switching and large breakdown field) before further engineering. In comparison to previous computational searches,[18,19] we expand the search space and focus on multinary ($n > 2$, where n is the number of chemical elements) wurtzite-type compounds.

To identify suitable candidates in a computationally accessible manner, we utilized the intrinsic breakdown field (E_b) and energy barrier for switching (ω_s) in single crystals as search parameters. The actual dielectric breakdown and ferroelectric switching mechanisms are expected to be more complicated based on contributions from impurities, defects, field inhomogeneities, etc.,[20,21] but the calculated E_b and ω_s represent their respective upper limits. Therefore, ω_s and E_b provide the relative tendencies to switch and to experience breakdown among different candidates. With these two calculated material properties and using AlN as the reference material, we identified several candidates that should demonstrate polarization switching before dielectric breakdown, and the most promising ones are Mg_2PN_3, Li_2SiO_3, Li_2GeO_3, and $MgSiN_2$. We identify unique switching pathways and intermediate non-polar structures for multinary (ternary and above) compounds. These pathways are distinct from the commonly assumed wurtzite-hexagonal-wurtzite switching pathway for binary compounds in the literature.[11,22–24] Furthermore, our calculated results of switching barriers provide systematic evidence across different chemistries for two qualitative design principles — ionicity and bond strength (Figure 1). These fundamental materials knobs can be tuned for future materials discovery and further engineering of candidates to have lower switching barrier and thus, lower coercive field.

2 Results and Discussion

2.1 Candidate Materials with Low Switching Barriers and High Breakdown Fields

The defining feature of ferroelectricity is that the spontaneous polarization needs to be switchable under an applied electric field.[10,25] The major challenge that prevents wurtzite-type ferroelectrics — or any polar material — from being switchable is that increasing electric field can cause dielectric breakdown before switching. To a first order, the coercive field is proportional to the switching barrier in units of energy density.[26] Therefore, we perform a computational search for candidates with higher

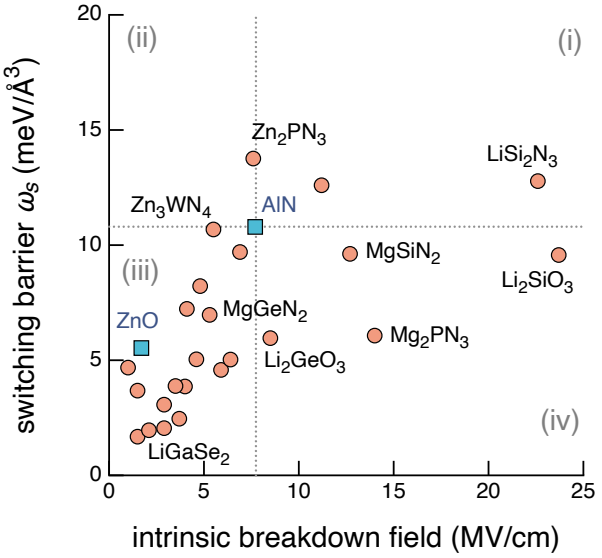

Fig. 2 Comparing calculated switching barriers to intrinsic dielectric breakdown fields of 24 candidates and 2 references compounds.

intrinsic dielectric breakdown fields (E_b) and lower switching barrier (ω_s) than the reference wurtzite materials like AlN and ZnO. Pure AlN and ZnO are not ferroelectrics at room temperature but they represent materials that have the potential to be—in fact, have been—further engineered, e.g., via alloying.[12–15]

Specifically, what distinguishes our work from previous computational searches[18,19] are that we used solid-state nudged elastic band method (SS-NEB) to calculate the switching barrier and we estimate the intrinsic breakdown field, which is a critical property for ferroelectrics. SS-NEB is known to predict lower and more physical switching barrier than the traditional NEB method since it allows more degrees of freedom, i.e. allows changes in cell volume and shape.[26] Moreover, our search focuses on multinary wurtzite-type compounds and includes sulfides and selenides in addition to nitrides and oxides, which allows us to deduce more general design principles that are applicable across chemistries.

Within a search space of 399 tetrahedral structures from the Inorganic Crystal Structure Database (ICSD), we identified 117 wurtzite-type structures (see Section 4.1 for details). Figure 2 compares E_b and ω_s of 24 multinary candidates that have thermodynamically stable wurtzite-type structures with c/a values less than 1.603 (AlN c/a). We also included AlN and ZnO as reference materials, and 9 newly-discovered wurtzite-type nitrides,[27] where the c/a criterion was not imposed. For switching barrier, instead of the commonly used unit of eV/f.u., we used eV/Å^3 for the following reasons. First, the coercive field depends on the energy density (eV/Å^3) directly.[25] Moreover, when comparing multinary compounds with different stoichiometries, the choice of the unit of eV/f.u. overestimates the barriers for compounds with higher number of atoms per f.u. and thus, leads to qualitatively different ranking (Fig. S1 in comparison to Figure 2).

From a bird's eye view, Figure 2 shows that wurtzite-type compounds with larger intrinsic breakdown fields generally have larger switching barriers. Such correlation showcases the diffi-

culty of searching for candidates with lower switching barriers but higher intrinsic breakdown fields. Fortunately, for compounds with similar E_b, their ω_s can still vary by two to three times. This observation makes the search possible and suggests that factors other than E_b (which predominately depends on the electronic band gap) may be important for the switching barrier.

Using AlN as a baseline, there are four quadrants regarding the likelihood to demonstrate ferroelectric switching: (i) higher E_b and higher ω_s, (ii) lower E_b and higher ω_s, (iii) lower E_b and lower ω_s, and (iv) higher E_b and lower ω_s. Figure 2 shows that there are a few oxides (Li_2SiO_3 and Li_2GeO_3) and nitrides ($MgSiN_2$ and Mg_2PN_3) within quadrant (iv), which is the search target region and the quadrant with highest likelihood of ferroelectric switching. In comparison, Zn_2PN_3 in quadrant (ii) has the lowest likelihood to demonstrate ferroelectric switching due to a combination of larger switching barrier and lower breakdown field than AlN.

Compounds in the quadrant (i) and (iii) are also potential candidates as demonstrated by ZnO (in quadrant iii) and particularly, by the $Zn_{1-x}Mg_xO$ alloy.[28] $LiSi_2N_3$ in quadrant (i) has slightly larger ω_s (by ~2 meV/Å^3) but its E_b is almost three times the estimated value for AlN. Generally speaking, for compounds within quadrant (i) and (iii), we expect increasing likelihood to demonstrate ferroelectric switching with closer proximity to the search target region. Overall, the broader search space leads to a large set of multinary compounds that can have higher E_b and lower ω_s than baseline materials like AlN and ZnO.

2.2 Existing Design Principle for Switching Barrier

Previous studies on wurtzite-type alloy ferroelectrics support the wurtzite c/a lattice parameter ratio as a key empirical descriptor for switching behavior in wurtzite-type ferroelectrics — lower the c/a value, lower the switching barrier (coercive field).[10,29] However, recent works have started to challenge its validity. We have recently identified the importance of ionicity of metal-anion bonds for describing the switching barrier in wurtzite-type ferroelectrics.[30] Recent studies have shown that the coercive field decreases with increasing B concentration in $Al_{1-x}B_xN$ alloy while the wurtzite c/a values are independent of the B concentration.[12] Similar findings have been reported for $Zn_{1-x}Mg_xO$ alloy where c/a remains constant. Since these studies focus only on alloys derived from AlN or ZnO, the generalizability of wurtzite c/a value as universal predictor remains unclear.

Since our computational search space includes multinary compounds and is *not* limited to the ideal wurtzite structure, our results provide a great opportunity to examine the validity of wurtzite c/a value as a predictor for switching barrier. Our computational search for multinary wurtzite-type compounds with lower switching barriers still utilized the wurtzite c/a as a descriptor. However, we further revisited its validity using calculated switching barriers for those candidates with low c/a values. The barriers are calculated with generalized solid-state nudged elastic band method (see methods for details).

Figure 3 shows the relationship between switching barrier and wurtzite c/a value for 24 candidates and 2 reference binary

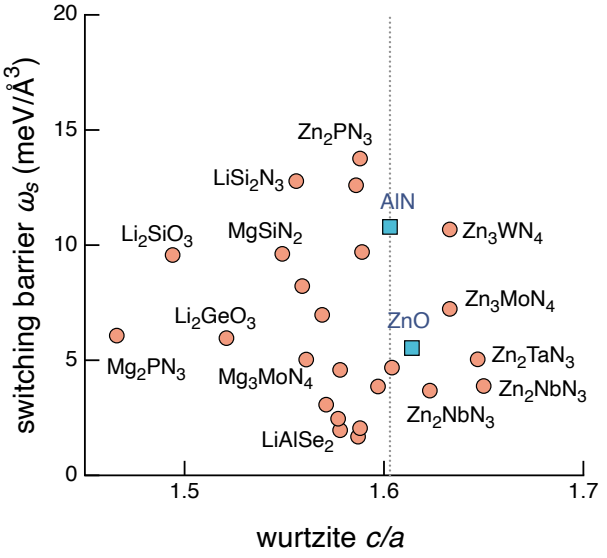

Fig. 3 Calculated switching barrier (ω_s), based on SS-NEB energy barrier, for 24 candidates and 2 references compounds (AlN and ZnO). The vertical dashed line indicates the AlN wurtzite c/a value of 1.603. The switching barriers, based on SS-NEB calculations, show no significant correlation with wurtzite c/a lattice parameter ratio.

wurtzite materials (AlN and ZnO). We calculate the wurtzite c/a value based on DFT relaxed structures and the group-subgroup symmetry relations discussed by Breternitz et al.[31] Figure 3 clearly shows that there is no significant correlation between switching barrier and wurtzite c/a. Using AlN as a reference point, the switching barrier can either increase or decrease with smaller c/a value. Therefore, our results show that wurtzite c/a lattice parameter ratio is not a good descriptor of switching barrier across different chemistries. However, it is worth noting that c/a value remains a practical descriptor for engineering a single compound via alloying since c/a generally correlates with local bond ionicity and ionic displacement, which are the emerging design principles for switching barriers.[30] Further discussion can be found in the following section.

2.3 Emerging Design Principles for Switching Barriers

The results in Figure 3 not only disprove wurtzite c/a value as a good descriptor for switching barrier but also support two emerging design principles — ionicity and bond strength. Figure 3 shows that the conventional wurtzite c/a value is a not a good descriptor for switching barrier across different chemistry groups. Figure 4 still supports the correlation within certain chemistry groups. Using Zn_2PN_3 and Mg_2PN_3, and Zn_3MoN_4 and Mg_3MoN_4 as example pairs, smaller c/a values correlate with smaller switching barriers. However, we want to emphasize that the c/a value is not the cause but the consequence of local bond ionicity.[30] In other words, it is the more ionic nature of Mg-N bonds than Zn-N bonds that gives rise to lower switching barrier (and lower c/a) for wurtzite-type candidates containing Mg than the ones with Zn (Figure 4).

In addition, Figure 3 shows that softer chemical bonds also leads to smaller switching barriers. Overall, sulfides and se-

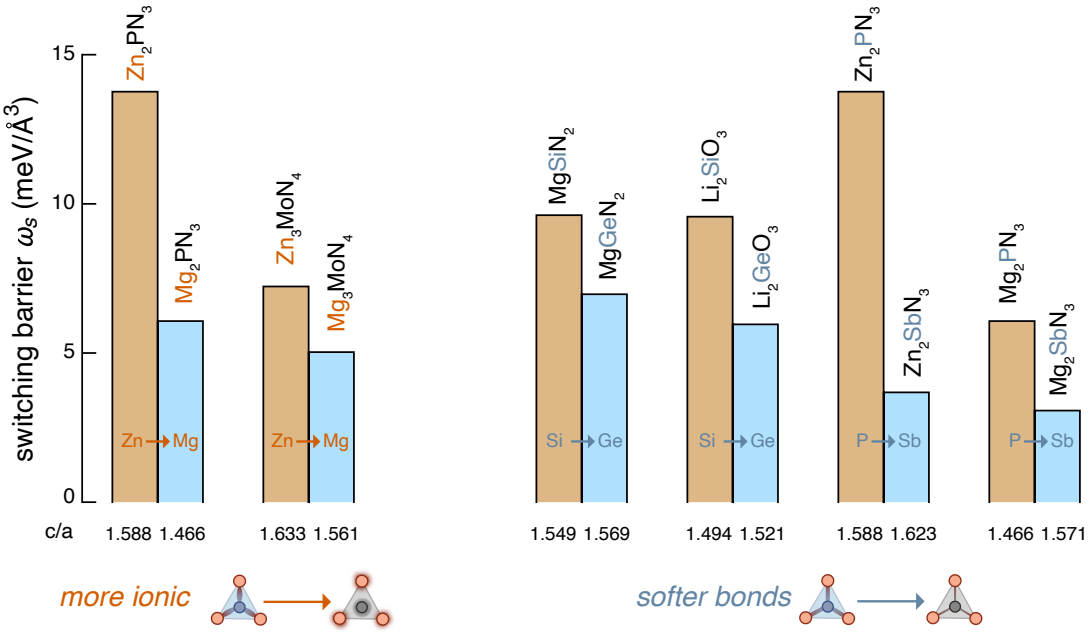

Fig. 4 Switching barrier (ω_s) of materials pairs selected to demonstrate the two emerging design principles – bond ionicity and softness. More ionic cation-anion bonds (e.g., Zn → Mg) reduces ω_s, while softer and more polarizable cation-anion bonds (e.g., P → Sb) also lead to reduced ω_s. However, bond ionicity and softness are not completely independent materials properties (Figure S3).

lenides, which generally form softer (more polarizable) bonds than oxides and nitrides, have lower switching barriers. This is consistent with the chemical intuition that cations move more easily and the atomic volumes are larger for materials with softer chemical bonds. Besides, with two nominal cations in ternary wurtzite-type compounds, the same trend can be seen for, e.g., Zn_2MN_3 chemistry (M = P, Sb, Nb, Ta). Sb, Nb, and Ta, which generally form softer cation-N bonds than P, give rise to smaller switching barriers (Figure 4). Similarly, $MgGeN_2$, $LiGe_2N_3$, Li_2GeO_3 has lower switching barriers than $MgSiN_2$, $LiSi_2N_3$, Li_2SiO_3, respectively, which is consistent with the chemical intuition that Ge forms more polarizable bonds with O and N atoms than Si.

To achieve the engineering goal of enabling ferroelectric switching in wurtzite-type compounds, we need not only low switching barriers but also sufficiently high dielectric breakdown fields, which predominantly depends on the electronic band gap (Section 4.2). Therefore, we further qualitatively examined how these two design principles affect the electronic band gap and the indication for dielectric breakdown field. Using the known $Zn_{1-x}Mg_xO$ system as an example, Mg-O bonds are more ionic than Zn-O bonds and at the same time MgO has larger electronic band gap. As a result, alloying ZnO with MgO leads to smaller coercive fields and larger band gaps.[28] In comparison, for $Al_{1-x}Sc_xN$, even though Sc-N bonds are more ionic than Al-N bonds,[30] rocksalt ScN has a relatively small band gap of ~1 eV.[32] Therefore, alloying leads to not only smaller coercive fields but also smaller band gaps. Based on these observations, one can engineer a compound further via alloying in a way that lowers the switching barrier and enhances the breakdown field. The ideal alloying strategy is to substitute cations with same valency (oxidation state) cations that form more ionic bonds with the anion.

From the bond strength perspective, since softer materials generally have smaller band gaps, exemplified by comparing selenides and sulfides to oxides, careful trade off is needed to avoid significant decrease in electronic band gaps and therefore, reduction in breakdown fields. Furthermore, bond ionicity and strength are not fully independent materials properties. Figure S3 compares the switching barrier of the material pairs in Figure 4 as a function of their bulk modulus, which is a measure of bond strength. Changing bond ionicity will simultaneously affect bond softness and band gap, with the latter directly affecting the breakdown field. Therefore, how to balance switching barrier and dielectric breakdown field remains highly nontrivial, and a descriptor that can simultaneously correlate with smaller switching barrier and larger electronic band gap is desirable for future investigations.

2.4 New Switching Mechanism and Non-polar Structure

The current understanding of polarization switching in tetrahedral ferroelectrics is largely based on studies on wurtzite-type alloys derived from AlN[10,26,33] and ZnO,[28] in which the switching is assumed to proceed via the wurtzite-hBN-wurtzite pathway, as shown in Fig. 5 (a), under external electric field.[11,22–24]

But a recent computational study,[34] which uses the NEB method, on $Al_{1-x}B_xN$ identified a switching mechanism that undergoes a pathway in which the β-BeO structure is the non-polar intermediate structure. Unlike the commonly assumed non-polar hBN-like structure, which is a saddle point in the transformation pathway, this β-BeO structure is a local minimum along the pathway (metastable). Recent experimental evidence suggests that $Al_{1-x}B_xN$ undergoes a phase transformation during switch-

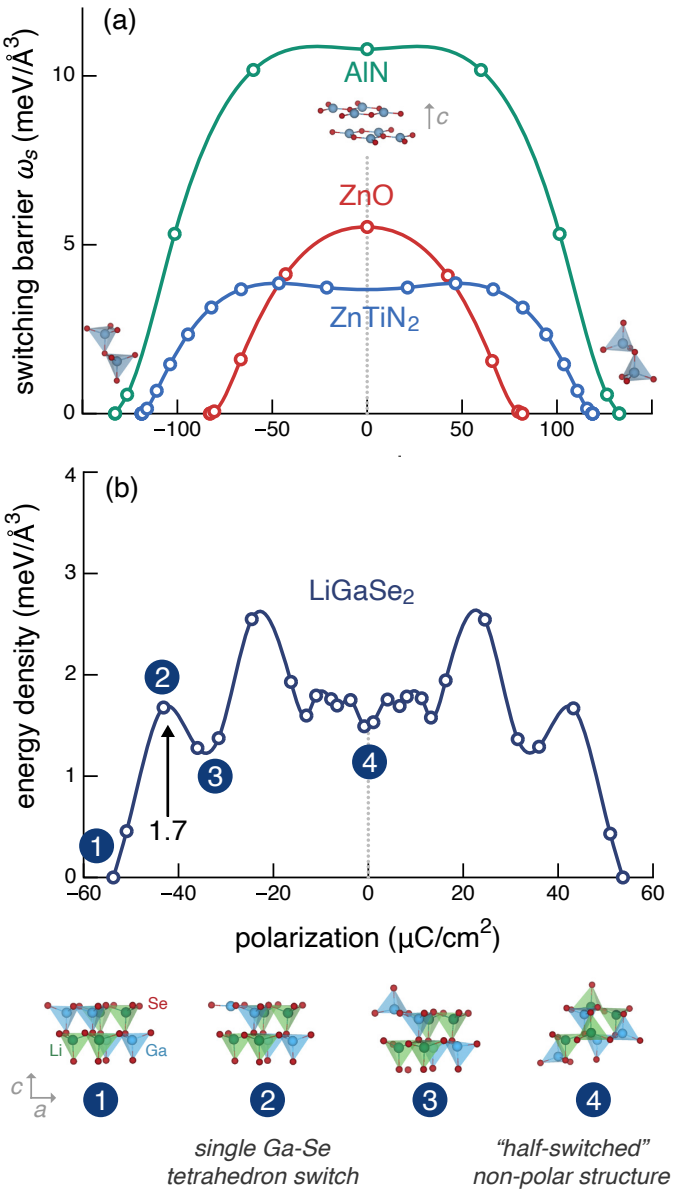

Fig. 5 Switching barrier ω_s as a function of polarization for two switching mechanisms. Solid curves are cubic spline fits to the data points obtained from SS-NEB calculations. The switching barriers are indicated by arrows for ZnO and $LiGaSe_2$. (a) Homogeneous switching: AlN and ZnO, which are the baseline materials, are used to demonstrate homogeneous switching. The intermediate hBN-like structure of AlN is shown as inset. $ZnTiN_2$ is a ternary compound that exhibits homogeneous switching (b) $LiGaSe_2$, which has the lowest switching barriers, is used to demonstrate the individual switching mechanism. Crystal structures along the switching pathway are shown, including the "half-switched" non-polar intermediate structure.

ing, where the intermediate structure is not the hBN-like structure.[35] Instead, the intermediate structure is an average non-polar, metastable structure consisting of anti-polar arrangements of wurtzite motifs when viewed along the [100] direction. Among other things, these finding could suggest that increasing chemical complexity (beyond binary wurtzites) can lead to different switching pathways, but this idea requires further investigation.

Multinary wurtzite-type ordered compounds share some similarity with AlN-based alloys in a way that cations with different ionicities and radii cause distortion from ideal wurtzite structure and give rise to different potential energy landscapes. For the 24 multinary candidates studied here, only two of them, $ZnTiN_2$ and Mg_3MoN_4, follow the commonly assumed wurtzite-hBN-wurtzite switching pathway. In comparison, we find that the rest of 22 wurtzite-type compounds follow a new switching pathway shown in Figure 5(b). We use $LiGaSe_2$, which has the lowest switching barrier, as an example to demonstrate the new pathway but the same feature as detailed below applies to all 22 candidates.

Before proceeding, we must define a consistent terminology to aid our explanation. Since all of the compounds in this study have a single anion and multiple cations, we define the tetrahedral structural unit ("wurtzite motif" in Ref. 35) according to the cation. Thus, when we say that a cation tetrahedron is oriented 'up', that means the polarization axis is vertical (along [001]) and that the nearest anion that sits directly on the axis with the cation is above the cation; if the same tetrahedron were oriented 'down', the cation would be below the anion basal plane, and the nearest c-axis-aligned anion would be below this cation.

The key difference of the new pathways from the wurtzite-hBN-wurtzite pathway lie not only in the non-polar intermediate structures but also the atomic scale switching processes. Unlike the known hBN-like non-polar structure, new non-polar structures that the SS-NEB method identifies using the primitive cell have half of the cation tetrahedra of the same type pointing in one direction along the polarization axis while the other half pointing to the opposite direction (crystal structures in Figure 5b). Among these new non-polar structures, some (e.g. $LiGaSe_2$ in Fig. S2) share similarity with the β-BeO structure recently identified,[34,35] while some are completely new (e.g. $LiAlS_2$ in Fig S2). In all these structures, since half of the cation tetrahedra are switched and on average, have net zero polarization, we refer to them as "half-switched structures" (Figure 5b). The half-switched structures are metastable i.e., located in potential energy wells. The structures along the transformation pathway, including the new non-polar structures, are available on GitHub.[36]

Figure 5 also shows distinct switching processes between the known and new switching pathway. All the cation tetrahedra switch coherently at the same time for the known wurtzite-hBN-wurtzite pathway, while individual cation tetrahedra switch sequentially for the new pathway. Therefore, we refer to the known and new pathways as *homogeneous* and *individual* switching, respectively for the rest of the manuscript. The difference in pathways affects how the switching barriers are calculated. For homogeneous switching, the barrier is either the energy density difference between the wurtzite-type polar structure and the hBN-like non-polar structure (AlN, ZnO in Figure 5a) or the maximal energy density difference along the transformation pathway when the hBN-like non-polar structure is not the highest energy structure ($ZnTiN_2$ in Figure 5a). However, for individual switching, the switching barrier is the largest barrier defined by a valley and its adjacent peak toward the switching direction. The idea is that if an applied electric field is large enough to overcome the largest barrier, it is large enough to overcome all of the other barriers.

Overall, the prevalence of materials that follow some version

of a new switching pathway (individual switching in 22 out of 24 multinary compounds) supports the hypothesis that increased chemical complexity can lead to different switching pathways and reduced overall switching barriers. Further investigations into the underlying mechanisms are clearly needed but are beyond the scope of this manuscript.

2.5 Further Considerations

We acknowledge that the calculated switching barriers are only the upper limit for the actual switching mechanisms as they do not account for domain wall motion or any effects of defects. This limitation is known in the literature,[26,37] but we emphasize that the goal is not to quantitatively predict the coercive field but to qualitatively examine the required energy density to switch polarization. We also note that it is only very recently that domain walls have even been confirmed in these ferroelectric wurtzites,[7] and that both the structures of the imaged domain walls and the relatively low energy of intermediate states via the individual switching pathways we report here would represent incredibly high charge density structures according to classic domain wall models.[25,38] Thus, there is a clear need for additional study of domain walls in tetrahedral ferroelectrics.

Our DFT calculations represent switching barriers at zero temperature, but switching barriers are known to decrease with increased temperature experimentally[13,29] and theoretically.[25,26] On the other hand, increasing temperature has mixed effect on dielectric breakdown field since higher temperature generally gives rise to smaller electronic band gap but to stronger electron-phonon interactions, which help dissipate energy delivered via electric field.[39] Recent experimental observations in $Al_{0.84}Sc_{0.16}N$, $Al_{0.93}B_{0.07}N$, and AlN thin films show decreasing breakdown field with increasing temperature but its temperature dependency is significantly weaker than that of coercive field.[29] Therefore, just as was the case in experiments, we expect the margin between coercive and breakdown fields to increase with increased temperature and therefore, for the trends identified here to be the same or possibly exaggerated at finite temperatures.

3 Conclusions

In summary, we performed a computational search and identified novel wurtzite-type compounds that can integrate with existing tetrahedrally bonded semiconductors while exhibiting sufficiently small coercive fields. Utilizing crystal symmetry relationships among wurtzite and its derived structures, we focus on the search space of wurtzite-type multinary compounds, which extends previous searches on binary wurtzite structures both in chemistry and complexity. Using AlN and ZnO as references, we found that the larger search space opens up opportunity of finding new wurtzite-type materials with a smaller switching barrier while maintaining or even increasing intrinsic dielectric breakdown field. Specifically, we find that Mg_2PN_3, Li_2SiO_3, Li_2GeO_3, and $MgSiN_2$ are the most promising wurtzite-type compounds for future investigations. With switching barriers calculated by the solid-state nudged elastic band method for 24 multinary wurtzite-type compounds, we find that wurtzite c/a values have *no* significant correlation with switching barriers across different chemistries but could remain a useful descriptor of switching barrier within certain chemistry groups. Instead, our results support two emerging design principles to achieve lower switching barrier — higher ionicity and lower bond strength. Between them, ionicity can be a more promising parameter for future engineering of candidates, e.g., via alloying, since higher ionicity generally gives rise to larger electronic band gap, while softer materials generally have smaller band gap. Lastly, we find that the majority (>90 %) of the multinary wurtzite-type candidates prefer different switching pathways that go through new non-polar, metastable structures. Overall, further understanding of the underlying switching mechanisms, along with the two design principles identified here, has the potential for discovering and engineering multinary wurtzite-type ferroelectrics, which are promising for next-generation low-power computing.

4 Methods

4.1 Computational Search Workflow

The goal of the computational search was to find new wurtzite-type compounds that can have low switching barrier but high intrinsic breakdown field. A schematic of the computational workflow is shown in Figure 6. We performed a search for stoichiometric and ordered tetrahedrally-bonded structures (TBSs) from the Inorganic Crystal Structure Database (ICSD). The TBSs were identified using an automated procedure, where the coordination was calculated by determining the first nearest neighbors using the minimum distance approach, with a tolerance of 0.3 – 0.5 Å. Each atom in a TBS must have 4-fold coordination. Next, we checked to ensure that the tetrahedral bond angles are within $109.5 \pm 20^\circ$. The large tolerance (20°) on the bond angles accommodates the distorted tetrahedral structures. This procedure for identification of TBSs is similar to the one we used in Ref. 40. We identified 399 TBS, spanning binary (153), ternary (127), and quaternary (119) chemistries. We also considered 9 newly-discovered wurtzite-type nitrides,[27] some of which have been experimentally synthesized.[41] We utilized the known group-subgroup symmetry relations[31] to identify 117 wurtzite-type structures out of the 399 TBSs.

Motivated by the empirical observation that lower wurtzite c/a lattice parameter ratio leads to smaller coercive fields, we prescreened the 117 wurtzite-type structures from ICSD to identify initial candidates with $c/a < 1.603$ (AlN c/a). We should note here that we ultimately find wurtzite c/a is not a good descriptor for switching barriers across different chemistries (Section 2.2).

Next, we assessed the thermodynamic phase stability of the wurtzite-type structures through convex hull analysis. We considered competing phases from the ICSD to construct the convex hull. In most cases, the total energy of the competing phases were taken from the NREL Materials Database.[42] DFT relaxations of the remaining structures were performed with the plane-wave VASP code[43] using the Perdew-Burke-Ernzerhof (PBE) exchange correlation functional within the generalized gradient approximation (GGA).[44] The valence electrons were treated with the projector-augmented wave (PAW) method. A plane-wave energy

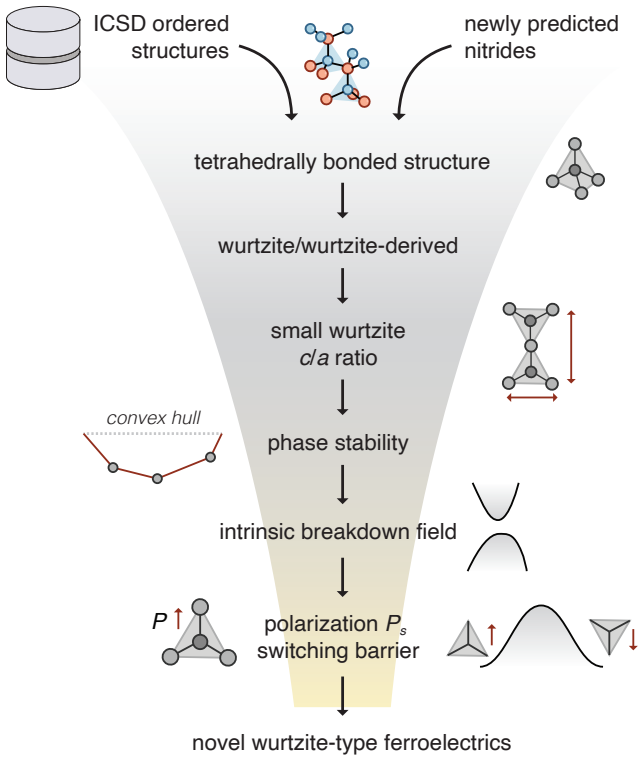

Fig. 6 Schematic of the computational workflow to identify novel wurtzite-type ferroelectric materials.

cutoff of 340 eV was used and automatically generated Γ-centered Monkhorst-Pack k-point grids were used to sample the Brillouin zone. The formation enthalpy of the wurtzite-type structures and competing phases was calculated from their DFT total energy and reference chemical potentials of the elemental phases. We used the fitted elemental-phase reference energies (FERE) as the reference chemical potentials, which has been shown to provide accurate predictions of formation enthalpy.[45] At the end, we downselected 24 wurtzite-type materials, including 9 new nitrides.

In the final step of the computational workflow, we employed a phenomenological model to estimate the intrinsic breakdown field,[46] and solid state-nudged elastic band (SS-NEB) method to calculate the polarization switching pathways and energy barriers.[47] Through this computational search, we identified four promising wurtzite-type ternary compounds as candidates with lower switching barriers and higher intrinsic breakdown fields compared to AlN.

4.2 Intrinsic Breakdown Field

We used a phenomenological model developed by Kim et al.[46] to estimate the intrinsic dielectric breakdown field E_b (in MV/m).

$$E_b = 24.442\ exp\left(0.315\sqrt{E_g \omega_{max}}\right). \quad (1)$$

where ω_{max} is the maximum phonon frequency (in THz) at Γ point of the Brillouin zone and E_g is the band gap (in eV). Semi-local DFT functionals are known to severely underestimate E_g. To address this issue, we calculated E_g of the candidate materials with DFT hybrid functional HSE06,[48] which generally provides better prediction of E_g. First, we relaxed the candidate wurtzite-type structures with HSE06 functional using the default 25% exchange fraction. Then, we calculated the electronic band structures, also with HSE06 functional, on a dense k-point grid such as $N \times n_{kpts} \simeq 8000$, where N is the number of atoms in the primitive cell and n_{kpts} is the number of k-points. For reference, a k-point density of 8000 translates to a $14\times14\times14$ k-point grid for the Si primitive cell. Future in-depth studies of specific candidate materials may employ beyond-DFT method such as the GW approximation for even more accurate E_g predictions.

4.3 Spontaneous Polarization

We followed the modern theory of polarization,[49,50] which uses the Berry phase approximation to calculate the electronic contribution to polarization. Specifically, we used the VASP 5.4.4. implementation and chose (0.25, 0.25, 0.25) crystal coordinates as the center of the reference frame for dipole calculations. The numerical parameters discussed in Section 4.1 were used for the Berry phase calculations. To calculate the ionic contribution to polarization, we used the atomic positions and assumed point charges; the calculation implemented in Pymatgen was used.[51] After the switching pathways were determined with SS-NEB, we used the algorithm implemented in Pymatgen to identify smooth polarization pathways and to calculate the polarization quanta.[51] In each case, we visually checked the smoothness of the polarization pathway since the automated algorithm in Pymatgen fails in certain cases.[51] In such cases, we manually identified smooth polarization pathways.

4.4 Switching Pathway and Energy Barrier

We applied the SS-NEB method[47] to determine the switching pathways between the polar and anti-polar structures, and to calculate the energy barrier (ω_s) along the pathways. We performed SS-NEB calculations using VASP Transition State Theory (VTST) tools developed by Henkelman and Jonsson.[52] Specifically, Vienna Ab-initio Simulation Package (VASP 5.4.4) and vtstcode-182 were used. First, we relaxed the polar wurtzite-type structure with DFT (Section 4.1). We then created the anti-polar structure by applying mirror reflection to the relaxed polar structure. By design, the anti-polar structure is relaxed and does not require further DFT relaxation. We created intermediate images through linear interpolation between the relaxed polar and anti-polar structures. Generally, such linear interpolation generates the common switching pathway via a hexagonal BN-like (hBN) non-polar structure. This linearly interpolated pathway is qualitatively similar to the converged SS-NEB pathways shown in Figure 5(a). We found that when the switching occurs via the hBN structure, SS-NEB calculations require only a small number of intermediate images (< 10) for convergence (forces $< 10^{-2}$ eV/Å). However, convergence of more complex switching pathways, such as the one shown for $LiGaSe_2$ in Figure 5b), requires a large number of intermediate images – roughly 2–8 times the number of cations in the simulation cell. As a result, SS-NEB calculations for the latter are computationally expensive but more accurate in un-

veiling unique switching mechanisms and non-polar intermediate structures. Lastly, since SS-NEB calculations allow cell degrees of freedom (similar to DFT structure relaxation), it is critical to update the Fourier grid after a certain number of ionic steps and use a large plane-wave cutoff energy for accurate calculation of stress and convergence of SS-NEB calculations.

Acknowledgements

Support for this work was provided by the National Science Foundation under Grant No. DMR-2119281 at the Colorado School of Mines, and by the Office of Science (SC), Office of Basic Energy Sciences (BES) as part of an Early Career Award at the National Renewable Energy Laboratory, operated by the Alliance for Sustainable Energy, LLC, for the US Department of Energy (DOE) under Contract No. DE-AC36-08GO28308. The work (energy calculations to understand switching mechanism) was also partially supported by the Department of Energy Basic Energy Sciences (BES), with additional support from Advanced Scientific Computing Research (ASCR), under program ERW6548. The research was performed using computational resources sponsored by the Department of Energy's Office of Energy Efficiency and Renewable Energy and located at the NREL. The views expressed in the article do not necessarily represent the views of the DOE or the U.S. Government.

Credit Statement

Cheng-Wei Lee: Investigation, Data Curation, Writing (Original Draft), Writing (Editing). **Naseem Ud Din**: Investigation, Data Curation, Writing (Editing). **Keisuke Yazawa**: Investigation, Writing (Editing). **Geoff L. Brennecka**: Conceptualization, Investigation, Writing (Editing), Project Administration. **Andriy Zakutayev**: Conceptualization, Investigation, Writing (Editing) **Prashun Gorai**: Conceptualization, Investigation, Data Curation, Writing (Editing), Supervision, Project Administration.

Conflicts of interest

There are no conflicts of interest to declare.

References

1 E. Masanet, A. Shehabi and J. Koomey, *Nature Climate Change*, 2013, **3**, 627–630.
2 A. S. G. Andrae and T. Edler, *Challenges*, 2015, **6**, 117–157.
3 E. Masanet, A. Shehabi, N. Lei, S. Smith and J. Koomey, *Science*, 2020, **367**, 984–986.
4 C. Freitag, M. Berners-Lee, K. Widdicks, B. Knowles, G. S. Blair and A. Friday, *Patterns*, 2021, **2**, 100340.
5 N. Jones *et al.*, *Nature*, 2018, **561**, 163–166.
6 T. Mikolajick, S. Slesazeck, H. Mulaosmanovic, M. H. Park, S. Fichtner, P. D. Lomenzo, M. Hoffmann and U. Schroeder, *J. Appl. Phys.*, 2021, **129**, 100901.
7 H. Mulaosmanovic, E. Chicca, M. Bertele, T. Mikolajick and S. Slesazeck, *Nanoscale*, 2018, **10**, 21755–21763.
8 E. T. Breyer, H. Mulaosmanovic, T. Mikolajick and S. Slesazeck, *Appl. Phys. Lett.*, 2021, **118**, 050501.
9 D. Ielmini and H. S. P. Wong, *Nat. Electron.*, 2018, **1**, 333–343.
10 S. Fichtner, N. Wolff, F. Lofink, L. Kienle and B. Wagner, *J. Appl. Phys.*, 2019, **125**, 114103.
11 C. E. Dreyer, A. Janotti, C. G. Van de Walle and D. Vanderbilt, *Phys. Rev. X*, 2016, **6**, 021038.
12 J. Hayden, M. D. Hossain, Y. Xiong, K. Ferri, W. Zhu, M. V. Imperatore, N. Giebink, S. Trolier-McKinstry, I. Dabo and J.-P. Maria, *Phys. Rev. Mater.*, 2021, **5**, 044412.
13 D. Drury, K. Yazawa, A. Zakutayev, B. Hanrahan and G. Brennecka, *Micromachines*, 2022, **13**, 887.
14 N. Wolff, M. R. Islam, L. Kirste, S. Fichtner, F. Lofink, A. Žukauskaitė and L. Kienle, *Micromachines*, 2022, **13**, 1282.
15 R. Guido, P. D. Lomenzo, M. R. Islam, N. Wolff, M. Gremmel, G. Schönweger, H. Kohlstedt, L. Kienle, T. Mikolajick, S. Fichtner and U. Schroeder, *ACS Appl. Mater. Interfaces*, 2023, **15**, 7030–7043.
16 X. Liu, J. Ting, Y. He, M. M. A. Fiagbenu, J. Zheng, D. Wang, J. Frost, P. Musavigharavi, G. Esteves, K. Kisslinger, S. B. Anantharaman, E. A. Stach, R. H. I. Olsson and D. Jariwala, *Nano Lett.*, 2022, **22**, 7690–7698.
17 K.-H. Kim, I. Karpov, R. H. Olsson and D. Jariwala, *Nat. Nanotechnol.*, 2023, **18**, 422–441.
18 H. Moriwake, R. Yokoi, A. Taguchi, T. Ogawa, C. A. J. Fisher, A. Kuwabara, Y. Sato, T. Shimizu, Y. Hamasaki, H. Takashima and M. Itoh, *APL Mater.*, 2020, **8**, 121102.
19 Y. Dai and M. Wu, *Sci. Adv.*, 2023, **9**, eadf8706.
20 A. K. Tagantsev, I. Stolichnov, N. Setter, J. S. Cross and M. Tsukada, *Phys. Rev. B*, 2002, **66**, 214109.
21 S. Zhukov, Y. A. Genenko, O. Hirsch, J. Glaum, T. Granzow and H. von Seggern, *Phys. Rev. B*, 2010, **82**, 014109.
22 F. Tasnádi, B. Alling, C. Höglund, G. Wingqvist, J. Birch, L. Hultman and I. A. Abrikosov, *Phys. Rev. Lett.*, 2010, **104**, 137601.
23 H. Moriwake, A. Konishi, T. Ogawa, K. Fujimura, C. A. Fisher, A. Kuwabara, T. Shimizu, S. Yasui and M. Itoh, *Applied Physics Letters*, 2014, **104**, 242909.
24 A. Konishi, T. Ogawa, C. A. Fisher, A. Kuwabara, T. Shimizu, S. Yasui, M. Itoh and H. Moriwake, *Applied Physics Letters*, 2016, **109**, 102903.
25 M. E. Lines and A. M. Glass, *Principles and Applications of Ferroelectrics and Related Materials*, Oxford University Press, 2001.
26 H. Wang, N. Adamski, S. Mu and C. G. Van de Walle, *J. Appl. Phys.*, 2021, **130**, 104101.
27 W. Sun, C. J. Bartel, E. Arca, S. R. Bauers, B. Matthews, B. Orvañanos, B.-R. Chen, M. F. Toney, L. T. Schelhas, W. Tumas, J. Tate, A. Zakutayev, S. Lany, A. M. Holder and G. Ceder, *Nat. Mater*, 2019, **18**, 732–739.
28 K. Ferri, S. Bachu, W. Zhu, M. Imperatore, J. Hayden, N. Alem, N. Giebink, S. Trolier-McKinstry and J.-P. Maria, *J. Appl. Phys.*, 2021, **130**, 044101.

29 W. Zhu, J. Hayden, F. He, J.-I. Yang, P. Tipsawat, M. D. Hossain, J.-P. Maria and S. Trolier-McKinstry, *Appl. Phys. Lett.*, 2021, **119**, 062901.

30 K. Yazawa, J. S. Mangum, P. Gorai, G. L. Brennecka and A. Zakutayev, *J. Mater. Chem. C*, 2022, **10**, 17557–17566.

31 J. Breternitz and S. Schorr, *Acta Crystallogr. A*, 2021, **77**, 208–216.

32 B. Biswas and B. Saha, *Phys. Rev. Mater.*, 2019, **3**, 020301.

33 K. Yazawa, J. Hayden, J.-P. Maria, W. Zhu, S. Trolier-McKinstry, A. Zakutayev and G. L. Brennecka, *Mater. Horiz.*, 2023, –.

34 Z. Liu, X. Wang, X. Ma, Y. Yang and D. Wu, *Applied Physics Letters*, 2023, **122**, 122901.

35 S. Calderon, J. Hayden, S. M. Baksa, W. Tzou, S. Trolier-McKinstry, I. Dabo, J.-P. Maria and E. C. Dickey, *Science*, 2023, **380**, 1034–1038.

36 https://github.com/prashungorai/papers/tree/main/2023/FEsearch.

37 M. Kruse, U. Petralanda, M. N. Gjerding, K. W. Jacobsen, K. S. Thygesen and T. Olsen, *npj Comput. Mater.*, 2023, **9**, 45.

38 X. L. Zhang, Z. X. Chen, L. E. Cross and W. A. Schulze, *J. Mater. Sci.*, 1983, **18**, 968–972.

39 Y. Sun, S. A. Boggs and R. Ramprasad, *Applied Physics Letters*, 2012, **101**, 132906.

40 P. Gorai, D. Krasikov, S. Grover, G. Xiong, W. K. Metzger and V. Stevanović, *Science Advances*, 2023, **9**, eade3761.

41 A. Zakutayev, S. R. Bauers and S. Lany, *Chem. Mater.*, 2022, **34**, 1418–1438.

42 *NREL Materials Database*, materials.nrel.gov.

43 G. Kresse and J. Furthmüller, *Phys. Rev. B*, 1996, **54**, 11169–11186.

44 J. P. Perdew, K. Burke and M. Ernzerhof, *Phys. Rev. Lett.*, 1996, **77**, 3865–3868.

45 V. Stevanović, S. Lany, X. Zhang and A. Zunger, *Phys. Rev. B*, 2012, **85**, 115104.

46 C. Kim, G. Pilania and R. Ramprasad, *Chem. Mater.*, 2016, **28**, 1304–1311.

47 D. Sheppard, P. Xiao, W. Chemelewski, D. D. Johnson and G. Henkelman, *J. Chem. Phys.*, 2012, **136**, 074103.

48 A. V. Krukau, O. A. Vydrov, A. F. Izmaylov and G. E. Scuseria, *J. Chem. Phys*, 2006, **125**, 224106.

49 R. D. King-Smith and D. Vanderbilt, *Phys. Rev. B*, 1993, **47**, 1651–1654.

50 R. Resta, *Rev. Mod. Phys.*, 1994, **66**, 899–915.

51 T. E. Smidt, S. A. Mack, S. E. Reyes-Lillo, A. Jain and J. B. Neaton, *Sci. Data*, 2020, **7**, 72.

52 G. Henkelman, B. P. Uberuaga and H. Jónsson, *J. Chem. Phys.*, 2000, **113**, 9901–9904.